Helicity of Peptoid Ions in the Gas Phase

Sébastien Hoyas[a,b] *Emilie Halin,*[b,c] *Vincent Lemaur,*[a] *Julien De Winter,*[b] *Pascal Gerbaux*[b]*, Jérôme Cornil*[a]*.

[a] Laboratory for Chemistry of Novel Materials, Center of Innovation and Research in Materials and Polymers, Research Institute for Science and Engineering of Materials, University of Mons, UMONS, 23 Place du Parc, 7000 Mons, Belgium

[b] Organic Synthesis & Mass Spectrometry Laboratory, Interdisciplinary Center for Mass Spectrometry (CISMa), Center of Innovation and Research in Materials and Polymers (CIRMAP), University of Mons - UMONS, 23 Place du Parc, 7000 Mons, Belgium

[c] Department of General, Organic Biomedical Chemistry, NMR and Molecular Imaging Laboratory, University of Mons - UMONS, 23 Place du Parc, 7000 Mons, Belgium.

Force field, helix, ion mobility, peptoids, secondary structure

Peptoids are attractive substitutes for peptides in several research areas, especially when they adopt a helical structure. The chain-size evolution of the secondary structure of the widely studied *N*spe peptoids is here analyzed by means of the ion mobility mass spectrometry technique increasingly used as a powerful analytical tool and is further supported by theoretical modelling. We conclude that the helical shape of the peptoids prevailing in solution is lost in gas phase by the need to screen the positive charge borne by the peptoid even though the collisional cross sections are close to the values expected for helical systems. We further illustrate that trend

line analyses predicting molecular shapes from fits of the size evolution of cross-sections can be very misleading since they critically depend on the range of polymerization degrees under study.

1. Introduction

Peptoids are poly-*N*-substituted glycines belonging to the peptidomimetic polymer family (**Scheme 1**).[1] The combination of the side chains that are appended to the backbone nitrogen atoms in peptoids (and not to the α-carbon atoms as in peptides) plays a key role for stabilizing the secondary structures, *i.e.*, helices, threaded-loop or ribbons, both in solution and in the solid state.[2–4] Over the years, synthetic protocols have been developed to introduce a wide variety of side chains for diverse applications (therapeutic, catalysis, …).[5–7] The most exploited secondary structure among all applications is the helix.[5,6,8] In many biological functions, the helical conformations are crucial for example in proteins as DNA binding motifs or as anchors to cross membranes,[9–12] or to prepare anti-microbial agents.[13] Helical peptoids could thus supplement peptides for a wide range of applications due to their increased stability against proteolysis.[1,5,14] For instance, they can be exploited as chiral catalytic sites for synthesis or as chiral resolving agent in chromatography.[6,15] Up to now, the most studied helical peptoids bear bulky and chiral side chains such as (*S*)-*N*-1-phenylethyl (*N*spe) (**Scheme 1**), which have been identified as two requirements to form well-defined helices.[16] While most structural studies on peptoid helices rely on similarities between the circular dichroism (CD) signature of peptides vs. peptoids and on nuclear magnetic resonance spectroscopy (NMR) to assess the secondary structure of peptoids in solution,[2,17] they rarely focused on mass spectrometry (MS) as a structural characterization tool,

except for a comparison made between cyclic poly(alanine) peptides and cyclic poly(sarcosine) peptoids.[18]

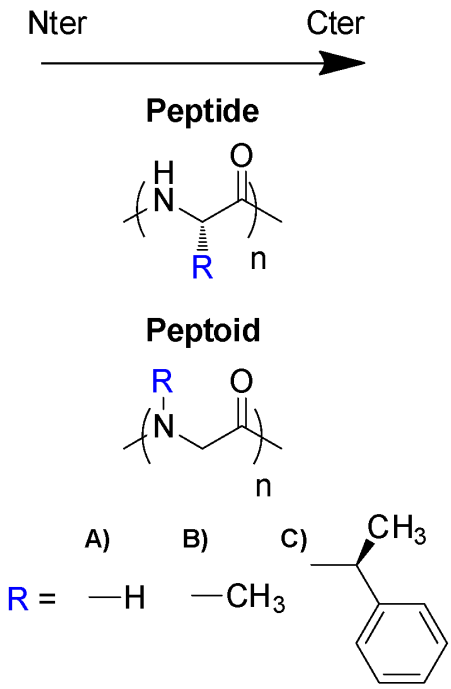

Scheme 1. General primary structure of peptides and peptoids, represented from the N to C terminus extremity. The side chains R considered are: **A**) hydrogen (glycine), **B**) methyl (*N*sar for peptoids and alanine for peptides) or **C**) (*S*)-1-phenylethyl (*N*spe for peptoids or 'spe' for peptides).

MS methods are typically exploited to elucidate the primary structure of peptoid compounds and validate synthetic routes.[19,20] In order to reach an additional analytical dimension, MS can be coupled to ion mobility (IM-MS). IM-MS allows differentiating gaseous ions based on their size, shape, charge and mass.[21] In such experiments, the drift time of ions passing through a mobility

cell filled with a buffer gas under the influence of an electric field is measured. For a given mass to charge ratio (m/z), extended ions will collide more with the gas than compact ions, and hence will remain longer in the mobility cell. The time spent in the cell is referred to as drift time and is directly related to the collision cross section, which reflects the 3D structure (and thus the conformation) of the ions.[22] In particular, ESI-IM-MS has been widely used to determine the conformation adopted by peptides/proteins and polymers.[23–25] A detailed structural assignment can be achieved by comparing the experimental collision cross sections to corresponding theoretical values computed on candidate structures obtained by experimental methods (X-ray crystallography or NMR),[26,27] or by computational chemistry.[25,28] Along the manuscript, the collision cross sections will be abbreviated using the current accepted notation.[21] The collision cross sections will be represented by Ω, with the experimental ones abbreviated as $^{TW}\Omega_{N2\square He}$ and the theoretical ones by $^{TM}\Omega_{He}$. A full description of the notation can be found **in SI**. It has to be recognized that IM-MS is not exempt of caveats. Indeed, the conformation of gaseous ionized molecules might significantly differ from the structure in solution due to structural rearrangements linked to the electrospray processes that involve ionization and desolvation.[29]

Another way to shed light on the gas-phase ion conformations, without relying on computational chemistry to generate the actual structures, is to study the evolution of Ω as a function of the mass-to-charge ratio (m/z) of homologous compounds. Such trend analyses are typically well-adapted to the study of polymers and homopeptides based on their intrinsic oligomer distributions.[30–32] For instance, singly charged polymer ions of different nature or protonated peptides often adopt globular conformations in the gas phase,[25,33–36] for which the evolution of Ω as a function of the mass (or the degree of polymerization (DP)) matches a power

law of $\Omega = A M^B$ where M is the molecular mass, B is around 2/3, *i.e.*, a characteristic value for a spherical evolution (see SI for details) and A is related to the ion density.[37] In this framework, polymer ions with $B < 2/3$ are considered as more compacted, while ions with $B > 2/3$ are more extended. Therefore, a value of B close to 1 is expected to be characteristic of extended structures growing linearly with the number of monomer units (or the mass). This trend line analysis has also been used for peptides, especially for protonated poly(alanine) ions, which fall into the trend line with B close to 2/3 as they adopt globular shapes in the gas phase.[34]

In the present communication, we investigate the conformation of singly charged *N*spe$_n$ (n = 3 – 15) peptoid ions in the gas phase. In particular, we analyze the experimental trend line ($^{TW}\Omega_{N2\square He}$ vs. M) to compare it to the theoretical trend line obtained for fully rigid hypothetic helical models. We chose to study these peptoids due to their propensity to form helical structures in solution[2,17] and to assess whether the helix is preserved in the gas phase. Moreover, we also investigate their conformation by performing molecular dynamics simulations on *N*spe ions in vacuum to mimic the experimental environment. Theoretical collision cross sections ($^{TM}\Omega_{He}$) values are then computed and compared to the experimental results.

2. Materials and Methods

Peptoid synthesis

All reactants and solvents are commercially available (VWR chemicals) and are used without any supplementary purification. *N*spe peptoids are synthesized using the solid-phase reaction protocol reported by Zuckermann and co-workers and used without further purification; all details are described elsewhere.[38–40] The *N*spe peptoids prepared for the present study were not extensively purified since they were only subjected to mass spectrometry analyses that, by definition, isolate ions in the gas phase based on their mass-to-charge ratio. Since, the

homopeptoids used in the present study were obtained by an efficient solid-phase protocol, their characterization is achieved based on the determination of the mass-to-charge ratio of the corresponding ions, $[M+H]^+$. A Table is added in the SI presenting all the investigated peptoids together with their mass parameters as neutrals and ions.

Ion mobility experiments

IM measurements are performed using a traveling wave ion mobility cell operated in N_2 as drift gas (Synapt G2-S*i*, Waters, U.K). The instrument description can be found elsewhere and the parameters are described in SI.[20] In TWIMS experiments, a calibration is required to convert drift times obtained in nitrogen into Ω. The calibration is carried out using singly charged polymers (poly(ethyleneglycol). This procedure is described elsewhere.[41] Reported $^{TW}\Omega_{N2□He}$ corresponds to the average of 3 replicates carried out at different wave velocities. Collision cross sections (experimental and theoretical) are reported using the currently accepted notation.[21]

Computational chemistry

Simulations were performed with Materials Studio 18.0,[42] using the PEPDROID force field parameter set.[43] For each polymerization degree, multiple starting geometries, carrying a proton on the terminal amine, were built (random and helical structures, with backbone and side chain dihedrals set as described by Armand *et al.*).[44] Partial charges are defined with the Gasteiger method based on the electronegativity of the bonded elements.[45] Each starting geometry is first optimized at the molecular mechanics level (MM) using the Conjugate Gradient algorithm with a 200 Å cut-off value for the non-bonded interactions so that none of them are neglected. Each optimized structure is then used as the starting point of a conformational search which is described in SI. Briefly, consecutive quenched dynamics are performed at different temperatures to obtain good starting geometries.[25] Then, the most stable one is used as the starting geometry

for two consecutive MD (NVT, 300 K, 10 ns, equilibration and production). From the production run, 100 conformations (frames saved every 0.1 ps) are submitted into the Collidoscope software using the 'trajectory method' (TM) algorithm with helium as colliding gas to calculate the collision cross sections ($^{TM}\Omega_{He}$).[46,47] Reported computed $^{TM}\Omega_{He}$ correspond to the average of 100 $^{TM}\Omega_{He}$ computed from the individual snapshots extracted from the last MD run.

3. Results and discussion

The *N*spe peptoids under investigation carry an amine moiety at their N terminus extremity (**Scheme 1**), which acts as the most basic site where the proton is located, whether in solution or in the gas phase. All the protonated *N*spe peptoids are transferred to the mass spectrometer gas phase via Electrospray ionization and further submitted to ion mobility separation. Every *N*spe peptoid ions are then characterized by monomodal arrival time distributions (ATD), see SI **Figure S1**. Beside the case of unresolved ions due to weak differences in $^{TW}\Omega_{N2-He}$, a monomodal narrow ATD indicates either that a unique ion structure is present or that multiple conformations interconverting faster than the timescale of the measurement (on the order of 10-20 ms) cannot be resolved.[48] The ATDs of each peptoid ion (*N*spe$_n$, n = 3 – 15) are converted into $^{TW}\Omega_{N2-He}$ (see experimental) and plotted as a function of mass (**Figure 1 D**). As reported in a recent paper, we prefer to represent the evolution of Ω with the mass rather than with the DP, since this allows to include the (0,0) point in the fitting process.[32] A power fit of the form $\Omega = A\,(M)^B$ yields a B value of 0.685, which is slightly larger than that expected for globular shaped ions (0.685 vs. 0.666) and much lower than the value of 1 expected for extended structures if the helical condensed phase structure is conserved upon transfer in the gas phase, as it is the case for polyalanine derivatives.[49] The difference between the measured B parameter (0.685) and the

typical evolution for a sphere (0.666) is rather weak, but significant as observed in **Figure 1 D**, thus suggesting that we might be in presence of other conformations in the gas phase.

To validate this hypothesis, we have computed the theoretical trend line ($\Omega \propto M^B$) for ideal helical *N*spe peptoids in the gas phase over a wide mass range. To do so, we calculate $^{TM}\Omega_{He}$ for hypothetic fully rigid helical structures of *N*spe ions of growing size (from DP 5 corresponding to the onset of formation of the helix until DP 60, **Figure 2 A**) without any optimization, with the dihedral angles based on those described by Armand *et al., i.e.,* similar to those of polyproline type I (ω = 0°, φ = -70°, ψ = 180°, χ_1 = 60°, χ_2 = -120°, definitions in SI, **Scheme S1**).[44] Such helical structures will be referred as 'peptoid helix' along the manuscript. From the trend line, we obtain a B parameter of 0.901 (**Figure 1 A**), which is strikingly different from 0.666 for globular shapes and 0.685 for the experimental data. Nonetheless, it must be emphasized that the mass range selected for the theoretical models is much larger than that spanned by the experiments. If we compute the B parameter for the theoretical data over the same range as in the experiment (up to DP 15), we obtain a value of 0.778 which is still higher than B_{exp} but also smaller than 0.901 found for the full series of model helices. When examining the evolution of the B parameter over different mass ranges, we observe an increase in B when extending the range (**Figure 1 B**). In order to calculate the B parameter evolution, we proceed as follows: starting at the origin, we determine the B parameter when increasing the mass range and plot the B value against the highest mass of the considered mass range. From these plots, we can extrapolate that B tends to the expected value of 1 for an infinite mass (see SI, **Figure S2**). We are thus led to the conclusion that the B parameter can be very misleading when analyzing a narrow range of DPs since its actual value is range dependent.

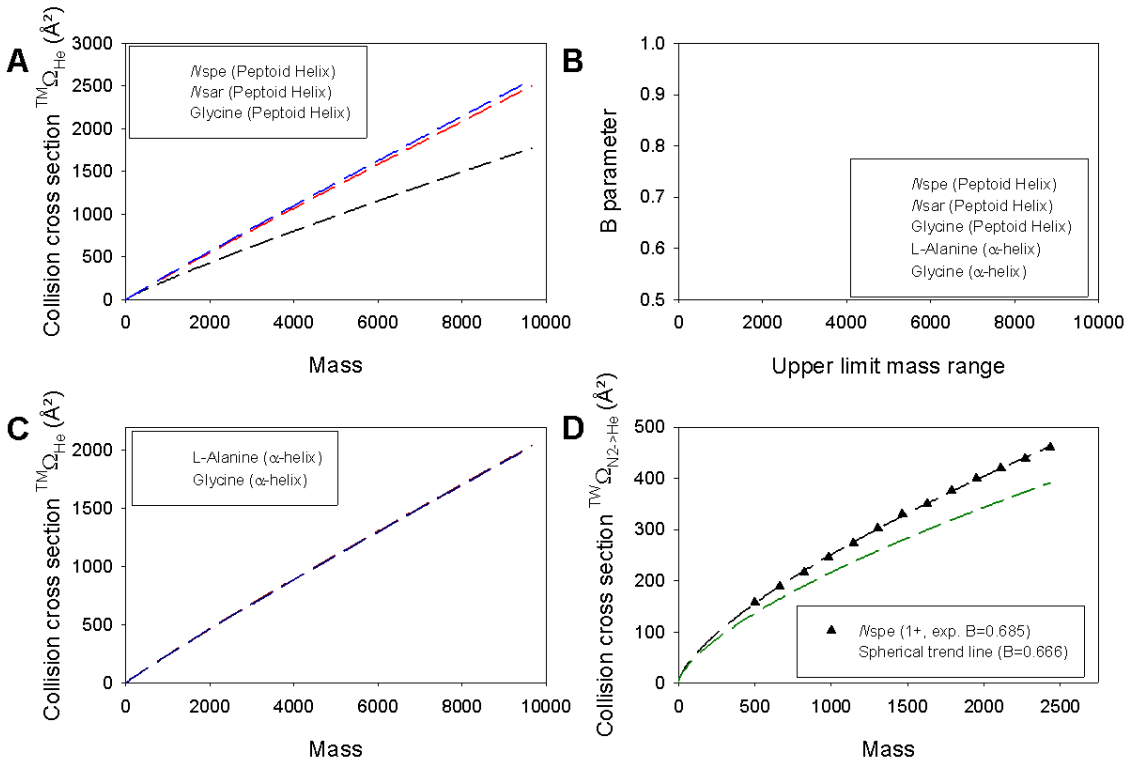

Figure 1. Theoretical trend lines of $^{TM}\Omega_{He}$ as a function of the mass for (**A**) ideal peptoid helices and (**C**) ideal peptide α-helices. (**B**) Evolution of the B parameter with the mass range for peptoids and α-helices with different side chains, as obtained by fitting the curves from plots (**A**) and (**C**). (**D**) Experimental trend line of $^{TW}\Omega_{N2\square He}$ for protonated *N*spe peptoid ions (black triangles) and theoretical trend line for a spherical evolution with the same mass and A parameter as those obtained extracted from the experimental trend line (empty green circles).

Based on this result, we wanted to further assess the influence of the nature of the side chain over the B parameter. We have thus extended our analysis by replacing the *N*spe side chains by methyl groups (*N*sar) or by hydrogen atoms (glycine) in new purely hypothetic structures (**Figure 1 A**). Due to the difference in mass of the side chains, and since we seek to compare their influence on the B parameter, *N*sar and glycine are spread over a larger DP range (from DP

5 to 132 and DP 5 to 168, respectively) to cover the same mass range than *N*spe peptoids. Interestingly, the theoretical B parameter is still higher than the 2/3 value of globular shapes (> 0.9) and is also higher for a given mass when the side chain is less sterically hindered ($B_{Nspe} < B_{Nsar} < B_{Glycine}$), reaching a value of almost 1 only in presence of hydrogen atoms (**Table 1**). Therefore, the evolution of B for these extended helices tends systematically toward 1, but at a different rate depending on the lateral substituents (**Figure 1 B**).

Table 1. A and B parameters obtained by fitting the theoretical $^{TM}\Omega_{He}$ vs. mass curves for the ideal hypothetic peptoid and peptide helices.

	A parameter	**B parameter**
Ideal hypothetic peptoid helix		
*N*spe	0.452 ± 0.021	0.901 ± 0.005
*N*sar	0.358 ± 0.007	0.964 ± 0.002
Glycine	0.364 ± 0.007	0.966 ± 0.002
Ideal hypothetic peptide α-helix		
Alanine	0.378 ± 0.012	0.936 ± 0.004
Glycine	0.368 ± 0.012	0.939 ± 0.010

In view of the close structural similarities between peptoids and peptides, we have also estimated the B parameter for purely hypothetic perfect protonated α-helices (ω = 180°, φ = -60°, ψ = -40°) bearing hydrogen atoms (glycine) and methyl moieties (L-alanine).[50] Such helices will

be described as 'peptide α-helix' in the rest of the manuscript. The B parameters for both trend lines are also higher than 0.666 but slightly lower that those obtained with the peptoid helices (**Figure 1 C & Table 1**). This difference finds its origin in the actual helical geometry; indeed, for a given mass, α-helices are more compacted than the peptoid helices, because of the specific combination of dihedral angles. Moreover, the helix base (2D helix projection) in peptides has a circular shape (**Figure 2 D & E, bottom**) with the hydrogen atoms or the methyl side chains tilted toward the inner core of the helix, while the peptoid helices feature a triangular base shape (**Figure 2 A, B & C, bottom**), with the side chains pointing out at the edges of the triangle. Consequently, the evolution of B as a function of the mass range also keeps increasing towards 1, as observed previously, though at a lower rate (**Figure 1 B)**. The variations in the B parameter can be rationalized by approximating a helix to a cylinder in which the height corresponds to the number of monomer units (or their mass) and the radius to the distance between the helix center and the atom lying the furthest away (**Figure S3**). For increasing helix size, the helix base (or its radius) is constant, while its height keeps increasing. If we analyze how the total surface and volume of a cylinder with a given radius evolves with increasing height, we find that the B parameter also tends towards 1 in both cases (see SI). However, for short radius, the evolution of B towards 1 is more rapid than for a larger radius, as it is the case when comparing the *N*spe peptoid helix and the *N*sar peptoid helix.

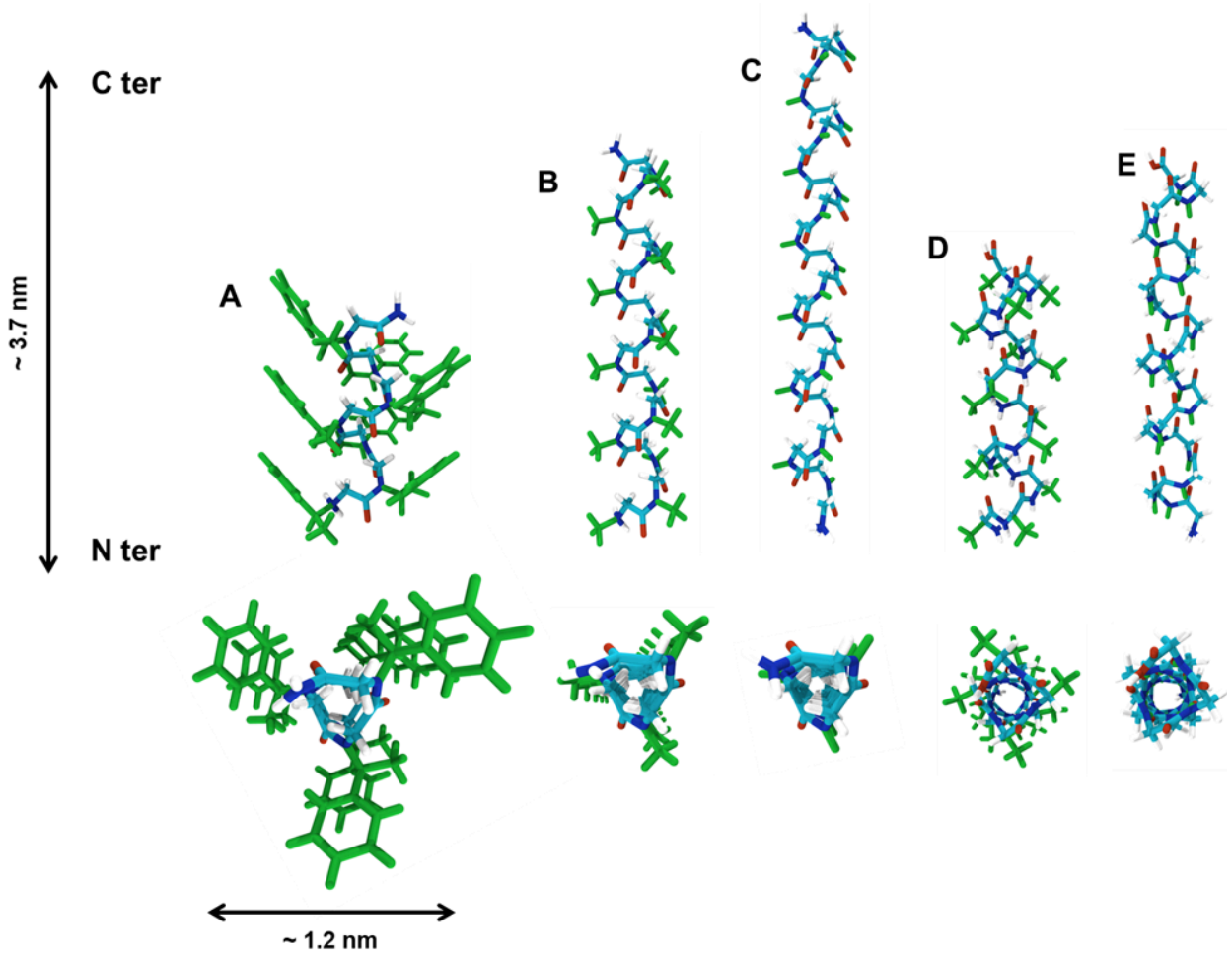

Figure 2. Ideal helix structures (viewed sidewise on top and along the helix axis from the C terminus at the bottom) for peptoids and peptides having about the same mass. (**A**), (**B**) and (**C**) are ideal peptoid helices (*N*spe, *N*sar, and glycine respectively), (**D**) and (**E**) are ideal α-helices (L-alanine and glycine, respectively). Side chains have been highlighted in green.

Due to the narrow range of DPs accessible experimentally and the associated B value different from 1, we cannot conclude that the protonated peptoids adopt helical shapes in the gas phase. This renders molecular modeling mandatory to suggest candidate structures and geometries. Accordingly, we have performed a conformational search by means of quenched MD simulations on the protonated *N*spe ions using the PEPDROID force field.[43] The most stable structures

obtained for each DP are clearly not spherical nor helical, as indicated by a trend line analysis. From DP 3 to 10, *N*spe ions adopt loop-like structures, with the ammonium in their center and the carbonyl groups pointing toward it to stabilize the charge by electrostatic interactions (**Figure 3 A, B**). This type of structure is reminiscent of the threaded loop structure adopted exclusively by the nonameric *N*spe peptoid in polar aprotic solvents, in which the terminal amine is protonated and allows for the formation of intramolecular H-bonds.[3] For DP comprised between 10 and 15, the additional monomer units do not take part in the charge solvation due to steric hindrance, but rather start forming a helical structure protruding out of the loop (**Figure 3 C**). The $^{TM}\Omega_{He}$ computed for the most stable structure of each DP are in very good quantitative agreement with the $^{TW}\Omega_{N2\square He}$ values (**Table S3**). As a result, the B parameter is also very similar for the two sets of data (0.685 in experiments vs. 0.697 in theory, see SI **Figure S4**). These results are consistent with an analysis carried out using trend lines, since a slight deviation of B from 0.666 is indeed enough to relate to a conformation different from spherical shaped objects and less compacted. The conformational ensemble of helices formed by *N*spe peptoids evidenced in solution[2] is thus not retained in the gas phase upon protonation. The main driving force for the structure collapse is the electrostatic stabilization of the charge in absence of solvation effects. Interestingly, the folding around the proton into loop-like structure is obtained at each polymerization degree, in contrast to the threaded loop structure dominating at DP 9 in solution when the peptoid is protonated.

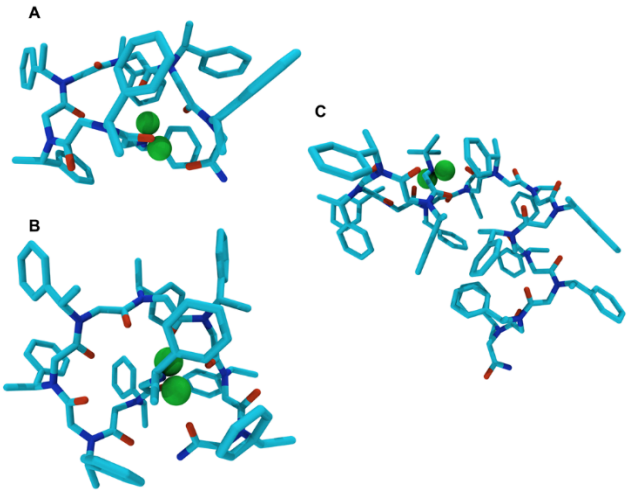

Figure 3. Most stable structures of *N*spe protonated ions obtained by successive quenched MD runs for (**A**) DP 7, (**B**) DP 9 and (**C**) DP 15. Hydrogens on the terminal ammonium are represented as green spheres while all other hydrogens were omitted for clarity.

Since the previous analysis on helices was made from ideal and frozen structures, we go one step further by considering possible slight structural rearrangements (side chain relaxation, structural changes around the ammonium) induced by the chain dynamics. To do so, we perform a single quenched MD at 300 K starting from the ideal helices for each DP (see SI, **Figure S5**). The relative energies of the relaxed helical structures are systematically higher than those of the loop structures described above (between 5 and 30 kcal/mol, see SI **Table S1**), thus giving further evidences that helices should not be observed in the experiment. In the narrow range of DPs under study, the B value obtained for relaxed structures (0.718) turns out to be close to that computed for the coiled structures (0.697), demonstrating the need for a computational support for unambiguous structural assignments.

4. Conclusions

Altogether, this communication sheds light on the structure of protonated peptoids revealed by IM-MS and points to the need of combining trend analysis and computational chemistry to identify the actual structures of the ions. Our calculations highlight that extended objects such as helices have their B parameter tending to 1 as their mass (or length) tends to infinity, but at a different rate depending on the chemical nature of the side chains. Since the B parameter extracted from trend line analyses depends on the range of DPs under consideration, much care should be taken when assigning shapes without the support of simulations of candidate structures. We evidence here that the non-retention of the helical structure of *N*spe peptoid ions when going from the solution to the gas phase is mainly caused by intramolecular charge solvation. Further work will be focused on peptoids having their N terminus capped to avoid the charge solvation process at this particular location. We are also working on peptoids bearing charged side chains to potentially promote the conservation of an extended structure in the gas phase.

ASSOCIATED CONTENT

Supporting Information

Details about the trend lines expected for spheres and cylinders, IM-MS notations, experimental details (calibration and analyses) and MD simulations can be found as supplementary material.

AUTHOR INFORMATION

Corresponding Author

* E-mail: Jerome.CORNIL@umons.ac.be (UMONS)

Present Addresses

†If an author's address is different than the one given in the affiliation line, this information may be included here.

Author Contributions

S.H.‡ and E.H.‡ have performed all calculations and experiments under the supervision of J.D.W. and V.L. All authors analyzed the set of data and contributed to the writing of the manuscript. All authors have given approval to the final version of the manuscript. ‡These authors contributed equally.

Funding Sources

Any funds used to support the research of the manuscript should be placed here (per journal style).

Notes

Any additional relevant notes should be placed here.

ACKNOWLEDGMENT

The work in the Laboratory for Chemistry of Novel Materials was supported by the Consortium des 'Equipements de Calcul Intensif' funded by the Fonds National de la Recherche Scientifique (FR-FNRS) under Grant No. 2.5020.11. The S²MOs lab is grateful to the FR-FNRS for continuing support. J.C. is an FNRS research fellow. S.H. and E.H. thank the "Fonds pour la Recherche Industrielle et Agricole" for their Ph.D. grants.

ABBREVIATIONS

Nspe, (*S*)-N-1-phenylethyl; MS, Mass Spectrometry; IM, Ion Mobility; CD, Circular Dichroism; NMR, Nuclear Magnetic Resonance; MD, Molecular Dynamics; CCS, Collision Cross Section; DP, Degree of Polymerization; Nsar, sarcosine; TW, Travelling Wave; TM, Trajectory Method; m/z, mass to charge ratio

REFERENCES

(1) Simon, R. J.; Kania, R. S.; Zuckermann, R. N.; Huebner, V. D.; Jewell, D. a; Banville, S.; Ng, S.; Wang, L.; Rosenberg, S.; Marlowe, C. K. Peptoids: A Modular Approach to Drug Discovery. *Proc. Natl. Acad. Sci. U. S. A.* **1992**, *89* (20), 9367–9371. https://doi.org/10.1073/pnas.89.20.9367.

(2) Armand, P.; Kirshenbaum, K.; Goldsmith, R. A.; Farr-Jones, S.; Barron, A. E.; Truong, K. T. V; Dill, K. A.; Mierke, D. F.; Cohen, F. E.; Zuckermann, R. N.; Bradley, E. K. NMR Determination of the Major Solution Conformation of a Peptoid Pentamer with Chiral Side Chains. *Proc. Natl. Acad. Sci.* **1998**, *95* (8), 4309–4314. https://doi.org/10.1073/pnas.95.8.4309.

(3) Huang, K.; Wu, C. W.; Sanborn, T. J.; Patch, J. A.; Kirshenbaum, K.; Zuckermann, R. N.; Barron, A. E.; Radhakrishnan, I. A Threaded Loop Conformation Adopted by a Family of Peptoid Nonamers. *J. Am. Chem. Soc.* **2006**, *128* (5), 1733–1738. https://doi.org/10.1021/ja0574318.

(4) Crapster, J. A.; Guzei, I. A.; Blackwell, H. E. A Peptoid Ribbon Secondary Structure. *Angew. Chemie - Int. Ed.* **2013**, *52* (19), 5079–5084. https://doi.org/10.1002/anie.201208630.

(5) Patch, J. A.; Barron, A. E. Helical Peptoid Mimics of Magainin-2 Amide. *J. Am. Chem. Soc.* **2003**, *125* (40), 12092–12093. https://doi.org/10.1021/ja037320d.

(6) Maayan, G.; Ward, M. D.; Kirshenbaum, K. Folded Biomimetic Oligomers for Enantioselective Catalysis. *Proc. Natl. Acad. Sci.* **2009**, *106* (33), 13679–13684. https://doi.org/10.1073/pnas.0903187106.

(7) Sun, J.; Zuckermann, R. N. Peptoid Polymers: A Highly Designable Bioinspired Material. *ACS Nano* **2013**, *7* (6), 4715–4732. https://doi.org/10.1021/nn4015714.

(8) Stringer, J. R.; Crapster, J. A.; Guzei, I. A.; Blackwell, H. E. Extraordinarily Robust Polyproline Type I Peptoid Helices Generated via the Incorporation of α-Chiral Aromatic N -1-Naphthylethyl Side Chains. *J. Am. Chem. Soc.* **2011**, *133* (39), 15559–15567. https://doi.org/10.1021/ja204755p.

(9) Berisio, R.; Vitagliano, L. Crystal Structure of the Collagen Triple Helix Model 3. *Protein Sci.* **2002**, 262–270. https://doi.org/10.1110/ps.32602.the.

(10) Ordway, G. A.; Garry, D. J. Myoglobin: An Essential Hemoprotein in Striated Muscle. *J. Exp. Biol.* **2004**, *207* (20), 3441–3446. https://doi.org/10.1242/jeb.01172.

(11) Doherty, A. The Helix-Hairpin-Helix DNA-Binding Motif: A Structural Basis for Non-Sequence-Specific Recognition of DNA. *Nucleic Acids Res.* **1996**, *24* (13), 2488–2497. https://doi.org/10.1093/nar/24.13.2488.

(12) Hildebrand, P. W.; Preissner, R.; Frömmel, C. Structural Features of Transmembrane Helices. *FEBS Lett.* **2004**, *559* (1–3), 145–151. https://doi.org/10.1016/S0014-5793(04)00061-4.

(13) Matsuzaki, K.; Sugishita, K. I.; Miyajima, K. Interactions of an Antimicrobial Peptide, Magainin 2, with Lipopolysaccharide-Containing Liposomes as a Model for Outer Membranes of Gram-Negative Bacteria. *FEBS Lett.* **1999**, *449* (2–3), 221–224. https://doi.org/10.1016/S0014-5793(99)00443-3.

(14) Miller, S. M.; Simon, R. J.; Ng, S.; Zuckermann, R. N.; Kerr, J. M.; Moos, W. H. Comparison of the Proteolytic Susceptibilities of Homologous L-Amino Acid, D-Amino Acid, and N-Substituted Glycine Peptide and Peptoid Oligomers. *Drug Dev. Res.* **1995**, *35* (1), 20–32. https://doi.org/10.1002/ddr.430350105.

(15) Wu, H.; Liang, T.; Yin, C.; Jin, Y.; Ke, Y.; Liang, X. Enantiorecognition Ability of Peptoids with α-Chiral, Aromatic Side Chains. *Analyst* **2011**, *136* (21), 4409. https://doi.org/10.1039/c1an15485k.

(16) Wu, C. W.; Sanborn, T. J.; Huang, K.; Zuckermann, R. N.; Barron, A. E. Peptoid

Oligomers with α-Chiral, Aromatic Side Chains: Sequence Requirements for the Formation of Stable Peptoid Helices. *J. Am. Chem. Soc.* **2001**, *123* (28), 6778–6784. https://doi.org/10.1021/ja003154n.

(17) Wu, C. W.; Sanborn, T. J.; Zuckermann, R. N.; Barron, A. E. Peptoid Oligomers with α-Chiral, Aromatic Side Chains: Effects of Chain Length on Secondary Structure. *J. Am. Chem. Soc.* **2001**, *123* (13), 2958–2963. https://doi.org/10.1021/ja003153v.

(18) Li, X.; Guo, L.; Casiano-Maldonado, M.; Zhang, D.; Wesdemiotis, C. Top-Down Multidimensional Mass Spectrometry Methods for Synthetic Polymer Analysis. *Macromolecules* **2011**, *44* (12), 4555–4564. https://doi.org/10.1021/ma200542p.

(19) Morimoto, J.; Fukuda, Y.; Kuroda, D.; Watanabe, T.; Yoshida, F.; Asada, M.; Nakamura, T.; Senoo, A.; Nagatoishi, S.; Tsumoto, K.; Sando, S. A Peptoid with Extended Shape in Water. *J. Am. Chem. Soc.* **2019**. https://doi.org/10.1021/jacs.9b04371.

(20) Halin, E.; Hoyas, S.; Lemaur, V.; De Winter, J.; Laurent, S.; Cornil, J.; Roithová, J.; Gerbaux, P. Side-Chain Loss Reactions of Collisionally Activated Protonated Peptoids: A Mechanistic Insight. *Int. J. Mass Spectrom.* **2019**, *435*, 217–226. https://doi.org/10.1016/j.ijms.2018.10.032.

(21) Gabelica, V.; Shvartsburg, A. A.; Afonso, C.; Barran, P.; Benesch, J. L. P.; Bleiholder, C.; Bowers, M. T.; Bilbao, A.; Bush, M. F.; Campbell, J. L.; Campuzano, J. L.; Causon, T.; Clowers, B. H.; Creaser, C. S.; De Pauw, E.; Far, J.; Fernandez-Lima, F.; Fjeldsted, J. C.; Gilles, K.; Groessl, M.; Hogan, S.; Kim, H. I.; Kurulugama, R. T.; May, J. C.; McLean, J. A.; Pagel, K.; Richardson, K.; Ridgeway, M. E.; Rosu, F.; Sobott, F.; Thalassinos, K.;

Valentine, S. J.; Wyttenbach, T. Recommendations for Reporting Ion Mobility Mass Spectrometry Measurements. *Mass Spectrom. Rev.* **2019**, *38* (3), 291–320. https://doi.org/10.1002/mas.21585.

(22) Lanucara, F.; Holman, S. W.; Gray, C. J.; Eyers, C. E. The Power of Ion Mobility-Mass Spectrometry for Structural Characterization and the Study of Conformational Dynamics. *Nat. Chem.* **2014**, *6* (4), 281–294. https://doi.org/10.1038/nchem.1889.

(23) Shelimov, K. B.; Clemmer, D. E.; Hudgins, R. R.; Jarrold, M. F. Protein Structure in Vacuo: Gas-Phase Conformations of BPTI and Cytochrome C. *J. Am. Chem. Soc.* **1997**, *119* (9), 2240–2248. https://doi.org/10.1021/ja9619059.

(24) Valentine, S.; Clemmer, D. H / D Exchange Levels of Gas Phase Cytochrome c Ions Excited in a Linear Quadrupole Ion Trap Outline • H / D Exchange • Results and Discussion H / D Exchange of Cytochrome c Linear Ion Trap – Time of Flight. **2002**, *0305* (02), 1–13.

(25) De Winter, J.; Lemaur, V.; Ballivian, R.; Chirot, F.; Coulembier, O.; Antoine, R.; Lemoine, J.; Cornil, J.; Dubois, P.; Dugourd, P.; Gerbaux, P. Size Dependence of the Folding of Multiply Charged Sodium Cationized Polylactides Revealed by Ion Mobility Mass Spectrometry and Molecular Modelling. *Chem. - A Eur. J.* **2011**, *17* (35), 9738–9745. https://doi.org/10.1002/chem.201100383.

(26) Jurneczko, E.; Barran, P. E. How Useful Is Ion Mobility Mass Spectrometry for Structural Biology? The Relationship between Protein Crystal Structures and Their Collision Cross Sections in the Gas Phase. *Analyst* **2011**, *136* (1), 20–28.

https://doi.org/10.1039/c0an00373e.

(27) D'Atri, V.; Porrini, M.; Rosu, F.; Gabelica, V. Linking Molecular Models with Ion Mobility Experiments. Illustration with a Rigid Nucleic Acid Structure. *J. Mass Spectrom.* **2015**, *50* (5), 711–726. https://doi.org/10.1002/jms.3590.

(28) Carroy, G.; Lemaur, V.; Henoumont, C.; Laurent, S.; De Winter, J.; De Pauw, E.; Cornil, J.; Gerbaux, P. Flying Cages in Traveling Wave Ion Mobility: Influence of the Instrumental Parameters on the Topology of the Host–Guest Complexes. *J. Am. Soc. Mass Spectrom.* **2018**, *29* (1), 121–132. https://doi.org/10.1007/s13361-017-1816-7.

(29) Duez, Q.; Metwally, H.; Konermann, L. Electrospray Ionization of Polypropylene Glycol: Rayleigh-Charged Droplets, Competing Pathways, and Charge State-Dependent Conformations. *Anal. Chem.* **2018**, *90* (16), 9912–9920. https://doi.org/10.1021/acs.analchem.8b02115.

(30) Marklund, E. G.; Degiacomi, M. T.; Robinson, C. V.; Baldwin, A. J.; Benesch, J. L. P. Collision Cross Sections for Structural Proteomics. *Structure* **2015**, *23* (4), 791–799. https://doi.org/10.1016/j.str.2015.02.010.

(31) Haler, J. R. N.; Morsa, D.; Lecomte, P.; Jérôme, C.; Far, J.; De Pauw, E. Predicting Ion Mobility-Mass Spectrometry Trends of Polymers Using the Concept of Apparent Densities. *Methods* **2018**, *144*, 125–133. https://doi.org/10.1016/j.ymeth.2018.03.010.

(32) Duez, Q.; Liénard, R.; Moins, S.; Lemaur, V.; Coulembier, O.; Cornil, J.; Gerbaux, P.; De Winter, J. One Step Further in the Characterization of Synthetic Polymers by Ion Mobility

Mass Spectrometry: Evaluating the Contribution of End-Groups. *Polymers (Basel).* **2019**, *11* (4). https://doi.org/10.3390/polym11040688.

(33) Henderson, S. C.; Li, J.; Counterman, A. E.; Clemmer, D. E. Intrinsic Size Parameters for Val, Ile, Leu, Gln, Thr, Phe, and Trp Residues from Ion Mobility Measurements of Polyamino Acid Ions. *J. Phys. Chem. B* **1999**, *103* (41), 8780–8785. https://doi.org/10.1021/jp991783h.

(34) Hudgins, R. R.; Mao, Y.; Ratner, M. a; Jarrold, M. F. Conformations of GlynH+ and AlanH+ Peptides in the Gas Phase. *Biophys. J.* **1999**, *76* (3), 1591–1597. https://doi.org/10.1016/S0006-3495(99)77318-2.

(35) Larriba, C.; Fernandez de la Mora, J. The Gas Phase Structure of Coulombically Stretched Polyethylene Glycol Ions. *J. Phys. Chem. B* **2012**, *116* (1), 593–598. https://doi.org/10.1021/jp2092972.

(36) Morsa, D.; Defize, T.; Dehareng, D.; Jérôme, C.; De Pauw, E. Polymer Topology Revealed by Ion Mobility Coupled with Mass Spectrometry. *Anal. Chem.* **2014**, *86* (19), 9693–9700. https://doi.org/10.1021/ac502246g.

(37) Ruotolo, B. T.; Benesch, J. L. P.; Sandercock, A. M.; Hyung, S.-J.; Robinson, C. V. Ion Mobility–Mass Spectrometry Analysis of Large Protein Complexes. *Nat. Protoc.* **2008**, *3* (7), 1139–1152. https://doi.org/10.1038/nprot.2008.78.

(38) Zuckermann, R. N.; Kerr, J. M.; Kent, S. B. H.; Moos, W. H. Efficient Method for the Preparation of Peptoids [Oligo(N-Substituted Glycines)] by Submonomer Solid-Phase

Synthesis. *J. Am. Chem. Soc.* **1992**, *114* (26), 10646–10647. https://doi.org/10.1021/ja00052a076.

(39) Tran, H.; Gael, S. L.; Connolly, M. D.; Zuckermann, R. N. Solid-Phase Submonomer Synthesis of Peptoid Polymers and Their Self-Assembly into Highly-Ordered Nanosheets. *J. Vis. Exp.* **2011**, No. 57, 1–7. https://doi.org/10.3791/3373.

(40) Lear, S.; Cobb, S. L. Pep-Calc.Com: A Set of Web Utilities for the Calculation of Peptide and Peptoid Properties and Automatic Mass Spectral Peak Assignment. *J. Comput. Aided. Mol. Des.* **2016**, *30* (3), 271–277. https://doi.org/10.1007/s10822-016-9902-7.

(41) Duez, Q.; Chirot, F.; Liénard, R.; Josse, T.; Choi, C.; Coulembier, O.; Dugourd, P.; Cornil, J.; Gerbaux, P.; De Winter, J. Polymers for Traveling Wave Ion Mobility Spectrometry Calibration. *J. Am. Soc. Mass Spectrom.* **2017**, *28* (11), 2483–2491. https://doi.org/10.1007/s13361-017-1762-4.

(42) Dassault Systèmes BIOVIA, Materials Studio, 18.0, San Diego: Dassault Systèmes, 2018. Dassault Systèmes BIOVIA, Materials Studio, 18.0, San Diego: Dassault Systèmes, 2018.

(43) Hoyas, S.; Lemaur, V.; Duez, Q.; Saintmont, F.; Halin, E.; De Winter, J.; Gerbaux, P.; Cornil, J. PEPDROID: Development of a Generic DREIDING-Based Force Field for the Assessment of Peptoid Secondary Structures. *Adv. Theory Simulations* **2018**, *1* (12). https://doi.org/10.1002/adts.201800089.

(44) Armand, P.; Kirshenbaum, K.; Falicov, A.; Dunbrack, R. L.; Dill, K. a; Zuckermann, R. N.; Cohen, F. E. Chiral N-Substituted Glycines Can Form Stable Helical Conformations.

Fold. Des. **1997**, *2* (6), 369–375. https://doi.org/10.1016/S1359-0278(97)00051-5.

(45) Gasteiger, J.; Marsili, M. A New Model for Calculating Atomic Charges in Molecules. *Tetrahedron Lett.* **1978**, *19* (34), 3181–3184. https://doi.org/10.1016/S0040-4039(01)94977-9.

(46) Ewing, S. A.; Donor, M. T.; Wilson, J. W.; Prell, J. S. Collidoscope: An Improved Tool for Computing Collisional Cross-Sections with the Trajectory Method. *J. Am. Soc. Mass Spectrom.* **2017**, *28* (4), 587–596. https://doi.org/10.1007/s13361-017-1594-2.

(47) Mesleh, M. F.; Hunter, J. M.; Shvartsburg, A. A.; Schatz, G. C.; Jarrold, M. F. Structural Information from Ion Mobility Measurements: Effects of the Long-Range Potential. *J. Phys. Chem.* **1996**, *100* (40), 16082–16086. https://doi.org/10.1021/jp961623v.

(48) Poyer, S.; Comby-Zerbino, C.; Choi, C. M.; Macaleese, L.; Deo, C.; Bogliotti, N.; Xie, J.; Salpin, J. Y.; Dugourd, P.; Chirot, F. Conformational Dynamics in Ion Mobility Data. *Anal. Chem.* **2017**, *89* (7), 4230–4237. https://doi.org/10.1021/acs.analchem.7b00281.

(49) Hudgins, R. R.; Jarrold, M. F. Helix Formation in Unsolvated Alanine-Based Peptides: Helical Monomers and Helical Dimers. *J. Am. Chem. Soc.* **1999**, *121* (14), 3494–3501. https://doi.org/10.1021/ja983996a.

(50) Lovell, S. C.; Davis, I. W.; Arendall, W. B.; de Bakker, P. I. W.; Word, J. M.; Prisant, M. G.; Richardson, J. S.; Richardson, D. C. Structure Validation by Cα Geometry: ϕ,ψ and Cβ Deviation. *Proteins Struct. Funct. Bioinforma.* **2003**, *50* (3), 437–450. https://doi.org/10.1002/prot.10286.

We assess whether the helicity of peptoids in solution can be probed by ion mobility mass spectrometry. We demonstrate with the help of theoretical modelling that peptoids actually adopt a loop-like geometry in the gas phase even though the measured collision cross sections are very similar to those expected for helices.